Corrosion Science 245 (2025) 112675

Contents lists available at ScienceDirect

Corrosion Science

journal homepage: www.elsevier.com/locate/corsci

Combinatorial discovery and investigation of the synergism of green amino acid corrosion inhibitors: Integrating high-throughput experiments and interpretable machine learning approach

Jingzhi Yang [a,b,c,1], Junsen Zhao [a,b,c,1], Xin Guo [a,b,c], Yami Ran [a,b,c], Zhongheng Fu [a,b,c,*], Hongchang Qian [a,b,c], Lingwei Ma [a,b,c], Patrick Keil [d], Arjan Mol [e], Dawei Zhang [a,b,c,*]

[a] Beijing Advanced Innovation Center for Materials Genome Engineering, Institute for Advanced Materials and Technology, University of Science and Technology Beijing, Beijing 100083, China
[b] Institute of Materials Intelligent Technology, Liaoning Academy of Materials, Shenyang 110004, China
[c] National Materials Corrosion and Protection Data Center, University of Science and Technology Beijing, Beijing 100083, China
[d] BASF Coatings GmbH, Münster 48165, Germany
[e] Department of Materials Science and Engineering, Delft University of Technology, Mekelweg 2, Delft 2628CD, the Netherlands

ARTICLE INFO

Keywords:
Corrosion inhibitor
High-throughput experiment
Machine learning
Amino acids

ABSTRACT

The discovery of synergistic strategies effectively improves the corrosion inhibition capability of amino acids. However, the wide variety of amino acid formulations and the time-consuming nature of corrosion tests make combinatorial discovery challenging to achieve. Herein, a library of 70 amino acids was created and tested in a high-throughput manner. Benefiting from a vast amount of labeled data of amino acid formulations, an interpretable machine learning approach was used to reveal the contribution of molecular features to inhibition performance of amino acids and the synergisms in the optimal formulation. The synergism was verified by electrochemical tests and quantum chemical calculations.

1. Introduction

The cleaning and maintenance of carbon steels in energy industries such as petroleum, natural gas, and coal strongly depended on industrial pickling and acid descaling methods. However, the carbon steels were prone to corrosion in the acid media, causing enormous safety concerns and economic burdens [1]. Appropriate corrosion mitigation technologies are essential for achieving a sustainable economy [2]. Among the various approaches to mitigate corrosion, the use of corrosion inhibitors is among the most effective methods due to their cost-efficient and user-friendly nature in practical applications [3,4]. Organic adsorption-type corrosion inhibitors are able to interact with metal surfaces through the ring structure and heteroatoms in the molecules, forming an adsorbed film to hinder the direct contact between the metal materials and corrosive media [5]. However, many organic corrosion inhibitors are criticized for being harmful to the environment [6]. The exploration of eco-friendly corrosion inhibitors from natural resources has thus attracted increasing attention in corrosion science and engineering communities.

Amino acids are essential nutrients for organisms and naturally exist in the cell walls of microorganisms and the protein components in the human body. Exogenous amino acids are generally non-toxic, biodegradable, and inexpensive [7]. Meanwhile, the amino and carboxyl groups along with a unique side chain of each amino acid provide various active sites to the molecules, endowing amino acids with a potentially significant corrosion inhibition performance [8–10]. Therefore, amino acids hold great promise as eco-friendly corrosion inhibitors. Kumar *et al.* investigated the corrosion inhibition mechanisms of cysteine (Cys), glutamic acid (Gla), glycine (Gly), and glutathione (Glt), indicating that the N, O, and S atoms of these amino acids could covalently bond with the Cu atoms on the surface [7]. Stimpfling *et al.* also demonstrated that Cys and phenylalanine (Phe) are promising

* Corresponding authors at: Beijing Advanced Innovation Center for Materials Genome Engineering, Institute for Advanced Materials and Technology, University of Science and Technology Beijing, Beijing 100083, China.
E-mail addresses: fuzhongheng@ustb.edu.cn (Z. Fu), dzhang@ustb.edu.cn (D. Zhang).
[1] These authors contributed equally.

https://doi.org/10.1016/j.corsci.2025.112675
Received 18 November 2024; Received in revised form 16 December 2024; Accepted 2 January 2025
Available online 7 January 2025

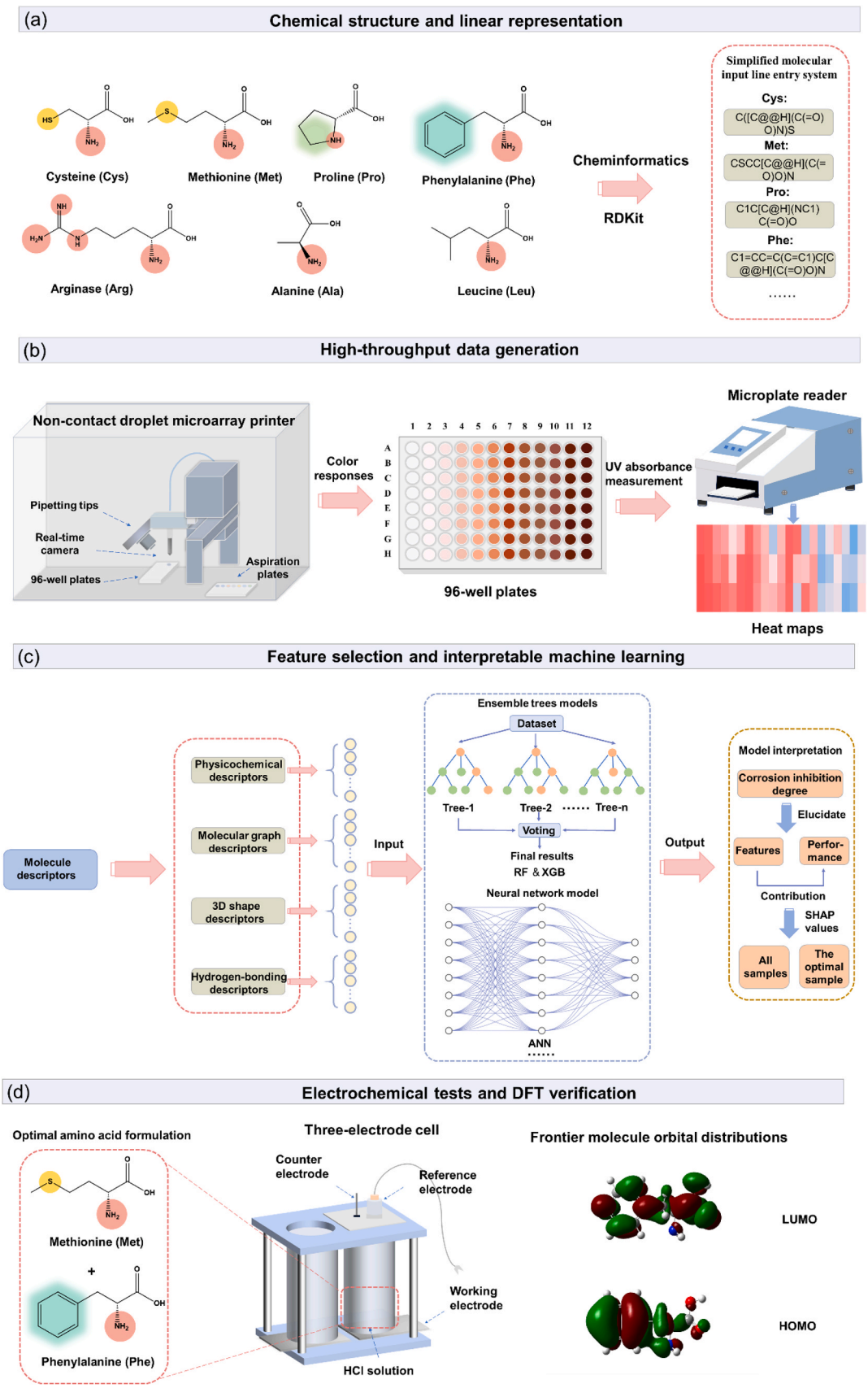

Fig. 1. Workflow of high-throughput experiments and machine learning integrating approach for the discovery and investigation of amino acid corrosion inhibitors.

corrosion inhibitors for aluminum alloy [9].

Although notable corrosion inhibition properties of some amino acids were claimed, the inhibition efficiencies of amino acids are relatively low compared to most traditional organic corrosion inhibitors, which may result from the inadequate electron-donating groups in their molecular structure [11]. The discovery of corrosion inhibitor mixtures with synergistic effects is an effective strategy to enhance the inhibition efficiencies of amino acids. For example, Zhang *et al.* discovered that the introduction of an imidazoline derivative significantly improved the inhibition effect of Cys for carbon steel. The synergistic effect was attributed to the compact inhibitor film formed by the initial adsorption of Cys and the subsequent adsorption of the imidazoline derivative [12]. Zhang *et al.* explored the inhibition performance of histidine/cysteine and thiourea corrosion inhibitor mixtures for carbon steel via experiments and calculation. The results indicated that the histidine and thiourea molecules could connect by strong intermolecular interactions, forming a compact film on the surface [13]. Prior research predominantly investigated the synergistic effect between amino acids and traditional organic corrosion inhibitors with relatively high toxicity. Potential synergies between amino acids were seldom reported.

Due to the wide diversity of amino acids, there are numerous possible formulations for amino acid combinations. Meanwhile, conventional electrochemical or weight loss measurements are time-consuming, making it difficult for the discovery of highly efficient amino acid combinations. Therefore, a high-throughput manner used for rapid discovery of individuals or optimal inhibitor mixtures has garnered escalating interest [14–18]. White *et al.* developed a multiple-channel method to simultaneously evaluate 10 corrosion inhibitors. This high-throughput approach achieved a high degree of reproducibility while improving the experimental efficiency up to 15 times [17]. Qiu *et al.* studied the synergistic corrosion inhibition behaviors of sodium fluoride/DL-malic acid mixtures with 24 concentrations via high-throughput visual identification. This strategy transformed the corrosion morphology into binary images for quantitative evaluation of metal corrosion degree [16]. Recently, our group developed a high-throughput experimental platform based on droplet microarrays to rapidly identify the optimal mixing ratio of benzotriazole and $Ce(NO_3)_3$ mixture. The enhanced corrosion inhibition of the mixtures resulted from the outstanding adsorption of benzotriazole on the CeO_2 layer [14]. In addition to the marked improvement of test efficiency, high-throughput experiments can generate a vast amount of foundational data that supports data-driven discovery and prediction. However, the relevant research on corrosion inhibitor mixtures using such an approach is still scarce.

In this work, high-throughput experiments and interpretable machine learning techniques were developed and integrated to discover the synergism between amino acid corrosion inhibitors. As shown in Fig. 1, the workflow primarily consists of four parts: i) the selection of amino acid molecules (see Section 3.1), ii) amino acid library screening via high-throughput experiments (see Section 3.2), iii) an interpretable machine learning approach for the performance evaluation (see Section 3.3), and iv) electrochemical tests and theoretical verification (see Sections 3.4 and 3.5). First, 7 kinds of amino acids with wide chemical diversity and corrosion inhibition potential were selected to create the data library. The library consists of 70 amino acid formulations assembled from diverse amino acid molecules with varying mixing ratios. A high-throughput experimental method based on automatic solution dispensing and color responses was used to efficiently evaluate the corrosion inhibition performances of various amino acid formulations. This method allows automated on-demand configuration of large quantities amino acid solutions in 96 well plates, and the inhibition degree of amino acids was rapidly evaluated by color responses to iron (Fe) ions produced during steel corrosion. In addition, representative molecular feature descriptors of amino acid inhibitors were identified, and an interpretable machine learning method was used to elucidate the contribution of these descriptors to the observed inhibition performance of amino acids. The machine learning results also highlighted the key descriptors that led to the synergism of the optimal amino acid formulation. Finally, the inhibition property and synergistic mechanism of optimal amino acid formulation were verified by electrochemical tests and quantum chemical calculations.

2. Materials and methods

2.1. Materials

Amino acids (L-Cysteine (L-Cys), L-Methionine (L-Met), L-Proline (L-Pro), L-Phenylalanine (L-Phe), L-Arginase (L-Arg), L-Alanine (L-Ala) and L-Leucine (L-Leu)) used in this work were purchased from Macklin Biochemical Co., Ltd. All chemicals were used as received without further purification. Q235 carbon steels were selected to study in this work because they were widely used in boilers, oil, and gas pipelines and very susceptible to acid media. The chemical composition (wt%) of the Q235 sample used in this work was C 0.19, Si 0.04, Mn 0.15, S 0.02, P 0.02, and Fe balance.

2.2. High-throughput solution configuration

The configuration of amino acid solution was achieved based on a non-contact droplet microarray printer (Nano-PlotterTMNP2.1, Germany). The printer was equipped with piezoelectric pipetting tips that allowed the software-controlled droplet automated dispensing. The pipetting tip aspirates the pre-prepared amino acid solutions from a 96-well plate. These solutions were transferred and mixed in a new 96-well plate. The automated washing and drying operations were triggered between the operations of dispensing different amino acid solutions. The dispensing task employing a 96-well plate, in which each well was loaded with 100 μL solution, could be accomplished within 1 hour. The solution configuration process was monitored by a stroboscope camera, which offered real-time imaging and calculated the precise volume of the droplet to guarantee the repeatability of experiments.

2.3. High-throughput corrosion assessment

The corrosion assessment was achieved by the color responses based on the reaction between Fe ions and sodium thiocyanate [15]. Briefly, the small Q235 steel samples (4 mm diameter, 0.08 μm Ra) were placed in the bottom of well-prepared 96-well plates. The 96-well plates were inclined at ~15 degrees to secure these small samples. During the corrosion process under HCl conditions, the uptake of a small amount of CO_2 from the air had a negligible effect on the pH of the test solutions in 96-well plates. After 1 day at 30°C in the dark, 100 μL 6 M HCl solution containing 0.05 M hexamethylenetetramine was added into each well followed by continuous sonication to completely dissolve the corrosion products. Afterwards, 20 μL solution was removed from each well and transferred to a new 96-well plate. 2 μL 30 wt% H_2O_2 was added into each well to convert the Fe^{2+} ions to Fe^{3+} ions. The solution in the plate was diluted by 1000 times, and then 50 μL solution from each well was pipetted to another plate. Subsequently, each well was added with 50 μL sodium thiocyanate solution (10 % w/w) to produce the $[Fe(SCN)]^{2+}$. A microplate reader (Multiskan FC, ThermoFisher Scientific) was used to spectrophotometrically measure the absorbance of each well at 480 nm [15,19]. The corrosion inhibition degree (ID_{corr}) was calculated by Eq. (1):

$$ID_{corr} = (1\text{-}E_{OD}/C_{OD}) \times 100\% \quad (1)$$

in which E_{OD} and C_{OD} were the OD_{480} values of the experimental group and control group, respectively. The typical digital images of the high-throughput solution configuration and corrosion assessment process are shown in Fig. S1.

Table 1
Setup of hyperparameters in grid search strategy for machine learning models.

Models	Hyperparameters	Values
ANN	Alpha	0.0001, 0.001, 0.01
	Learning_rate_init	0.001, 0.01, 0.1
	Max_iter	5000
	Tol	0.001, 0.01
XGB	Learning_rate	0.1, 0.5, 1
	N_estimators	100, 500
	Max_depth	3, 5, 7
SVR	K_range	[100,1000], step = 100
	K2_range	[0.01, 0.10], step = 0.01
RF	N_estimators	10, 100
	Min_samples_split	2, 5, 10, 20
	Min_samples_leaf	1, 5, 10
LR	None	None

2.4. Machine learning surrogate models

The machine learning models were trained by python package scikit-learn (version 0.20.1). Artificial neural network (ANN), extreme gradient boosting (XGB), support vector regression (SVR), random forest (RF), and linear regression (LR) algorithms were used to build the regression models based on the experimental results generated from our high-throughput corrosion experiments. These models demonstrate extensive diversity and can use different algorithms to identify complex patterns and relationships in large data sets. ANN was inspired by biological neural networks and composed of interconnected artificial neurons. ANNs learned by adjusting the weights and biases of the connections between neurons. XGB was developed based on a decision tree algorithm and was emphasized minimizing the loss function by iteratively fitting the residuals of label and model. SVR was suitable for regression problems. It tried to find the best fitting line or hyperplane in a high-dimensional space. RF was an ensemble learning method that operated by constructing a multitude of decision trees and each tree was trained on a different subset of the original data set. LR used the least square strategy to fit the linear relationships between input and output. A detailed description of the principles of these machine learning algorithms can be found at https://scikit-learn.org/. The hyperparameters of each model were tuned by a grid search strategy to improve the performance of models in the experimental data set (Table 1), The other hyperparameters remained at their default values. 80 % of the experimental results were chosen as a training set, while the residual 20 % were used as a test set to assess the accuracy of the model. This process was repeated 100 times with diverse training sets and corresponding test sets. The average values of root mean-squared error (RMSE) and coefficient of determination (R^2) of these 100 iterations were employed to evaluate the predictive capabilities of different regression models, using Eqs. (2) and (3), respectively.

$$\mathrm{RMSE} = \sqrt{\frac{1}{n}\sum_{k=1}^{n}(y_k - \tilde{y}_k)} \tag{2}$$

$$R^2 = 1 - \frac{\sum_{k=1}^{n}(y_k - \tilde{y}_k)^2}{\sum_{k=1}^{n}(y_k - \bar{y})^2} \tag{3}$$

in which n was the number of samples, y_k and $\tilde{y}_k$ were the experimental results and machine learning predicted results. A lower RMSE value and larger R^2 represent a higher accuracy of the model. The model with the best accuracy was chosen.

Shapley Additive exPlanations (SHAP) tools were used to interpret the machine learning model output. The SHAP analysis utilized a game-theoretic framework to link the optimal credit allocation with the explanations of the model prediction. In the SHAP analyses, each input feature is regarded as a contributor to the model output. SHAP analysis generated a SHAP value for each input feature, which indicates their quantitative contribution including the contribution importance (the value of SHAP) and the contribution direction (the positive or negative SHAP values).

2.5. Electrochemical tests

Electrochemical impedance spectroscopy (EIS) and potentiodynamic polarization (PDP) were carried out in a three-electrode cell in 0.1 M HCl solution. The working electrode was a Q235 steel sample, while a platinum sheet (1.0 cm^2 exposed area) and a saturated calomel electrode were used as the counter electrode and the reference electrode, respectively. The Q235 steel samples (60 × 40 × 3 mm^3) were abraded sequentially by 400, 800, and 1200 grit abrasives. The abraded samples were cleaned ultrasonically in ethanol and subsequently dried in the air before use. These samples were immersed in the amino acid solution for a period of time (~ 5 minutes) until a steady open-circuit potential (OCP) was reached. The EIS tests were performed at the OCP from 100 KHz to 10 MHz frequency with a 5 mV sinusoidal perturbation. The PDP measurements were scanned in a potential range of ± 250 mV versus with a scan rate of 0.5 mV/s. All experiments were performed at 30 ℃.

2.6. Quantum chemical calculations

Density functional theory (DFT) calculations were performed to evaluate the electronic interactions between methionine, phenylalanine inhibitor molecules, and carbon steel samples [20]. The corresponding theoretical parameters of the highest occupied molecular orbital (HOMO) and the lowest unoccupied molecular orbital (LUMO) of these molecules were calculated at B3LYP/6–31 g* level using Gaussian 09 software. The eigenvalues of HOMO (E_{HOMO}) and LUMO (E_{LUMO}) of molecules were also calculated.

3. Results and discussion

3.1. The selection of amino acids to create the data library

7 commercially available amino acids were selected to provide wide chemical diversity, including alkane chains of various lengths, heteroatoms in different chemical environments, linear and cyclic aliphatic structures, and aromatic moieties. Their chemical structure and linear representation are listed in Fig. 1a. These amino acids have demonstrated potential to mitigate metal corrosion (e.g., Ala and Leu for steel [10], Cys for zinc [21] and steel [13], Met and Arg for Fe [22], and Phe for magnesium alloy [23]). Moreover, these amino acids have extremely low biological toxicity, showing 10- to 50-fold lower median lethal dose (LD_{50}) values than some of the widely used organic corrosion inhibitors [24–29] (intraperitoneal injection, rat, data from 'Registry of Toxic Effects of Chemical Substances', Table 2).

Table 2
LD_{50} values of the selected amino acid monomers and some conventional organic corrosion inhibitors.

Amino acids	Cys	Met	Pro	Phe	Arg	Ala	Leu
LD_{50}, mg kg^{-1} (rat, intraperitoneal, RTECS)	1620	4328	5110	5287	16,000	>5000	5379
	BTA	CTAB	2AT-Me	MBT	MBI	8-HQ	DMAE
LD_{50}, mg kg^{-1} (rat, intraperitoneal, RTECS)	400	106	~200	100	200	43	234

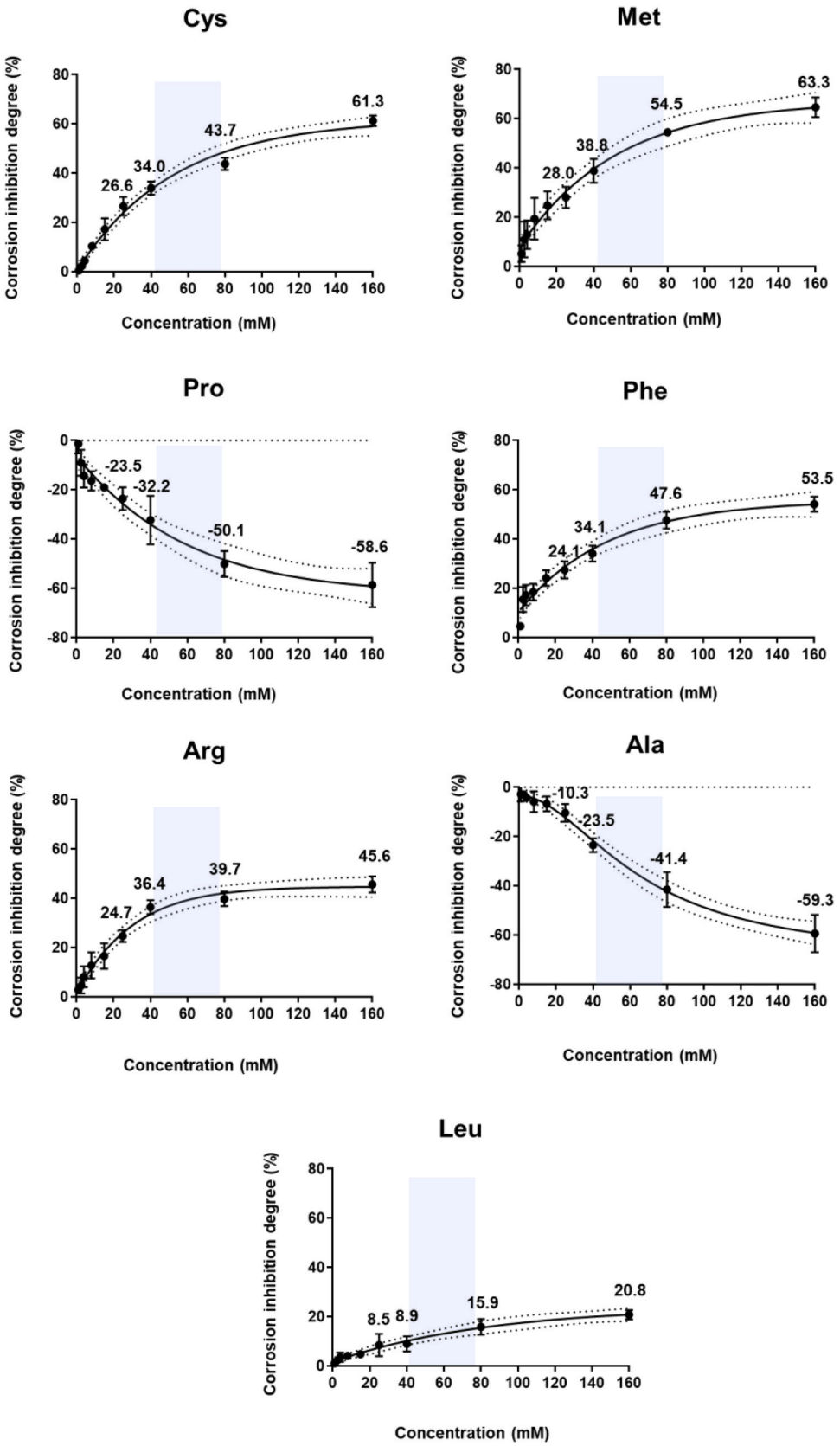

Fig. 2. The IDcorr values of the amino acid inhibitors as functions of concentrations. The curve started to flatten out after the concentration range in the blue area. The values represented the IDcorr values for different concentrations. Data are means ± SD ($n = 4$, SD indicates standard deviation).

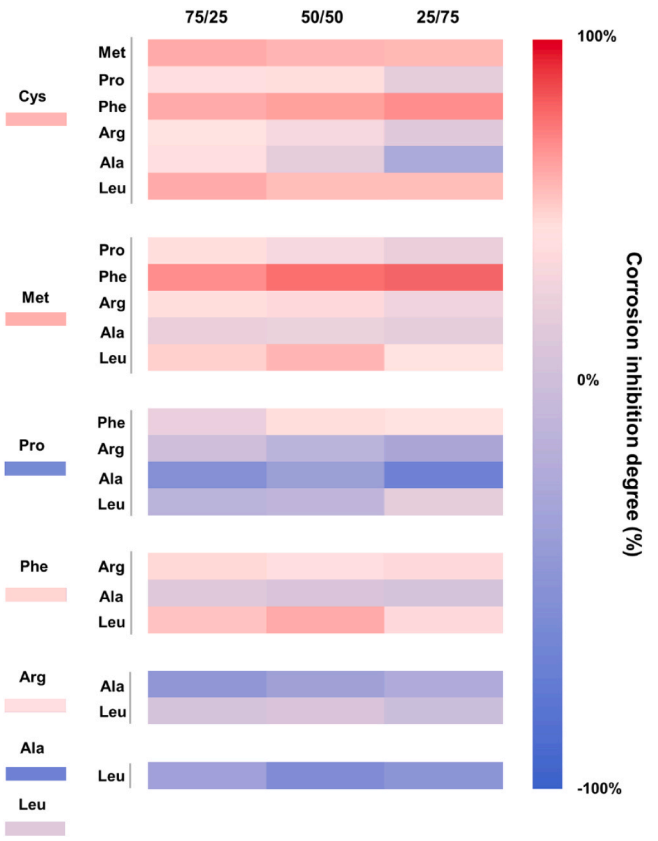

Fig. 3. Heat map of the IDcorr values of amino acids used alone and in combination based on high-throughput screening assays. The total concentration of amino acid mixtures used in this map was fixed at 160 mM. Data are means ($n = 4$).

3.2. Combinatorial screening of amino acid library

In order to study the corrosion inhibition behaviors of amino acid solutions at different concentrations, 63 kinds of amino acid solutions, involving 7 amino acids (Cys, Met, Pro, Phe, Arg, Ala, and Leu) and 9 concentrations (1, 2, 4, 8, 15, 25, 40, 80, and 160 mM), were first configured using the microarray printer. Subsequently, color responses were used to rapidly evaluate the corrosion inhibition performance of these amino acids (see Section 2.3, Eq. (1)). Although all of the tested amino acids have different pK_a values, their dissolution resulted in similar pH values of HCl solution. The high-throughput experimental results are shown in Fig. 2**.** 5 amino acids exhibited corrosion inhibition capabilities based on the given concentration range. Among these 5 amino acids, Cys and Met exhibited relatively high corrosion inhibition degrees (~63 %) for carbon steels. In general, the adsorption capacities of the organic inhibitors were attributed to the chemical structures of the inhibitor molecules and the surface properties of the metals. The S atom in the chemical structures of Cys and Met has lone electron pairs, which could generate additional coordination with the empty orbitals of Fe atoms, thereby enhancing the interaction between inhibitors and metal surfaces [30,31]. Phe and Arg also showed moderate levels of corrosion inhibition. The π-π stacking formed by overlapping *p*-orbitals of the benzene rings may help the adsorption of Phe molecules [32]. The N atoms in Arg enhance its inhibition performance [33]. Due to the inherent amino and carboxyl groups, Leu also exhibited a certain inhibition degree for carbon steels in HCl solution. Amino could adsorb onto metal surfaces by forming coordination bonds or hydrogen bonds, while carboxyl tended to form complex compounds with iron or iron ions. With their increasing concentration, the corrosion inhibition performances of these 5 amino acids were improved. This could be explained by an increasing number of adsorbed molecules on the metal surface at higher concentrations, leading to a denser surface coverage [34,35]. All 5 amino acids exhibited the highest corrosion inhibition degree at the concentration of 160 mM. The increase in the inhibition performance from 80 mM to 160 mM was relatively limited and leveled off compared to the inhibition effect for increasing concentration at lower concentrations. Compared to the increasing concentration, the discovery of a synergistic inhibiting strategy is expected to be a promising approach to further improve the inhibition performance of amino acids. The amino acids at 80 mM concentration were selected to study in combinations. In addition to the 5 amino acids that exhibited corrosion inhibition behavior, carbon steels were more severely corroded in the presence of the other 2 amino acids (Pro and Ala). This phenomenon could be explained that Pro and Ala molecules tend to adsorb in aggregation on the surface due to the extremely short C–C skeletal chain. Such a pattern resulted in various electrochemical activity regions on the metal surface, potentially accelerating the corrosion process [36]. The enhanced molecule–molecule interactions at higher concentrations may facilitate this aggregation [37,38].

The similar method was used to investigate the corrosion inhibition levels of 70 amino acids composed of binary combinatorial mixtures at 4 molar ratios (100:0, 75:25, 50:50, and 25:75). The results of this combinatorial discovery were summarized in the heat map (Fig. 3), where red and blue colors represent positive and negative IDcorr values, respectively. The deeper color represents the higher absolute value of the calculated IDcorr. Although the inhibition performance of amino acid mixtures laid between the two constituent amino acids in most cases, some mixtures exhibited superior inhibition capabilities compared to those of these amino acids used alone. The introduction of Phe, Met, Cys, and Leu demonstrated improved inhibition capabilities in different degrees (evidenced by the deeper red squares in the heat map). Among these, amino acid mixtures composed of 25 % Met and 75 % Phe exhibited the highest IDcorr values (81.85 %) among all amino acid mixtures. By comparison, the IDcorr values of 100 % Met and 100 % Phe were 63.25 % and 53.50 %, respectively. The synergism requires that the inhibition performance of a mixture surpasses the maximum measured inhibition performance of any single composition [39]. This definition is well applicable for the mixture system where the maximum measured inhibition concentrations (optimum concentrations) were determinate or the total concentrations were fixed. Therefore, a corrosion inhibitor mixture combining 25 % Met and 75 % Phe displayed the synergistic effect. For this condition, the synergistic parameter could be calculated by Eq. (4):

$$S = \frac{1 - \max\left(\eta_1^{opt}, \eta_2^{opt}\right)}{1 - \eta_{12}} \tag{4}$$

where η_1^{opt} and η_2^{opt} are the optimum inhibition performances of the single amino acid compounds 1 and 2, respectively. η_{12} is the inhibition performance of the optimal amino acid mixture. The IDcorr values were used to qualitatively evaluate the inhibition performance of amino acids in the high-throughput screening process. Therefore, the synergistic parameter of the 25 % Met and 75 % Phe mixture was determined to be 2.02.

3.3. Machine learning analysis

As a data-driven centric approach, machine learning is capable of "learning" from the experimental results and grasping the underlying relationship between the input and output [40–42]. A machine learning approach was established to understand the relationship between molecular features and the corrosion inhibition effect of the amino acids in this work. Searching for molecular feature descriptors that are strongly associated with the target property and integrating them into an appropriate machine learning algorithm could effectively improve the accuracy of a surrogate model. To identify such feature descriptors, we

Table 3
Feature descriptors and their representation used in this work.

Features	Descriptors	Representation
Physicochemical	LogP	Logarithm of octanol/water partition coefficient
	TPSA	A cumulative value of the polar areas
2D molecular graph	BalabanJ	Distance between atoms in a molecular graph
	BertzCT	Complexity of the bonding and distribution of heteroatoms
	HallKierAlpha	Polarity and charge density of molecules
3D molecular shape	InertialShapeFactor	Mass distribution and geometric center
	Asphericity	Degree that the shape of the molecule deviates from sphericity
	Eccentricity	Degree of asymmetry in molecular shape.
Hydrogen-bonding	HBA	Atoms available for hydrogen bonding donors
	HBD	Atoms available for hydrogen bonding acceptors

first considered the inherent physical and chemical properties of molecules, including hydrophilia, hydrophobicity, and polarity. These properties significantly influence the interaction between adsorbed film and carbon steel surface [43,44]. Moreover, the molecular structures mainly determined the corrosion inhibition performances of organic inhibitors [45,46]. Ma *et al.* found that the incorporation of 2D–3D molecular structural features improved the capability of the machine learning model to predict the corrosion inhibition performance of organic molecules [47]. Hydrogen bonding was another factor, which influenced the molecular interaction and the adsorption of corrosion inhibitors on the metal surfaces [19,32].

After comprehensive consideration, a feature descriptor set was computed for each amino acid molecule, composed of physicochemical descriptors (LogP and TPSA), 2D molecular graph descriptors (BalabanJ, BertzCT, and HallKierAlpha), 3D shape descriptors (InertialShapeFactor, Asphericity, and Eccentricity) and hydrogen-bonding descriptors (HBA and HBD). These descriptors are able to quantitatively describe the relevant features of amino acid molecules from multiple perspectives. Their simple representation was shown in Table 3. Detailed information of these descriptors can be found at https://rdkit.org/docs/search.html. All amino acid molecules were expressed by their simplified molecular input line entry system (SMILES) strings, which encode atomic connected order and chemical bond information in a succinct and standardized way. The SMILES strings defined digital file formats for the chemical information of molecules [48]. RDKit was used to convert the SMILES of amino acid molecules into feature descriptors [49]. Table 4 listed the specific value of each feature descriptor for each amino acid molecule in this work. Moreover, the descriptor-based feature set of the amino acid mixtures was generated by weighing the descriptor values of the corresponding constituents based on the molar ratio. This feature analysis facilitated to identify the relevant characteristics of individual amino acid molecules. Five regression models including ANN, XGB, SVR, RF, and LR were built based on the unique feature descriptor values (input) and high-throughput experimental IDcorr values (output) of 70 amino acids. The RMSE and R^2 were used to evaluate the prediction accuracy of the models. XGB model yielded the optimal regression performance with an RMSE value of 11.5 and an R^2 value of 0.90 (Fig. 4**a**). A large proportion of data points were located in the dashed line (Fig. 4**b**). Therefore, the XGB model was chosen to train the experimental dataset [50].

Table 4
Feature descriptor values of each amino acid used in this work.

	LogP	TPSA	BalabanJ	BertzCT	HallKier Alpha	InertialShape Factor	Asphericity	Eccentricity	HBA	HBD
Cys	−0.67	63.32	3.30	75.34	−0.22	0.0043	0.27	0.93	3	3
Met	0.15	63.32	3.27	96.96	−0.22	0.0048	0.54	0.98	3	3
pro	−0.18	49.33	2.35	96.60	−0.57	0.0071	0.40	0.96	3	2
Phe	0.64	63.32	2.58	258.49	−1.35	0.0044	0.58	0.99	3	3
Arg	−1.55	127.72	3.44	176.39	−1.30	0.0035	0.57	0.98	6	7
Leu	0.44	63.32	3.50	101.23	−0.57	0.0037	0.28	0.93	3	3
Ala	−0.58	63.32	3.26	59.81	−0.57	0.0070	0.23	0.91	3	3

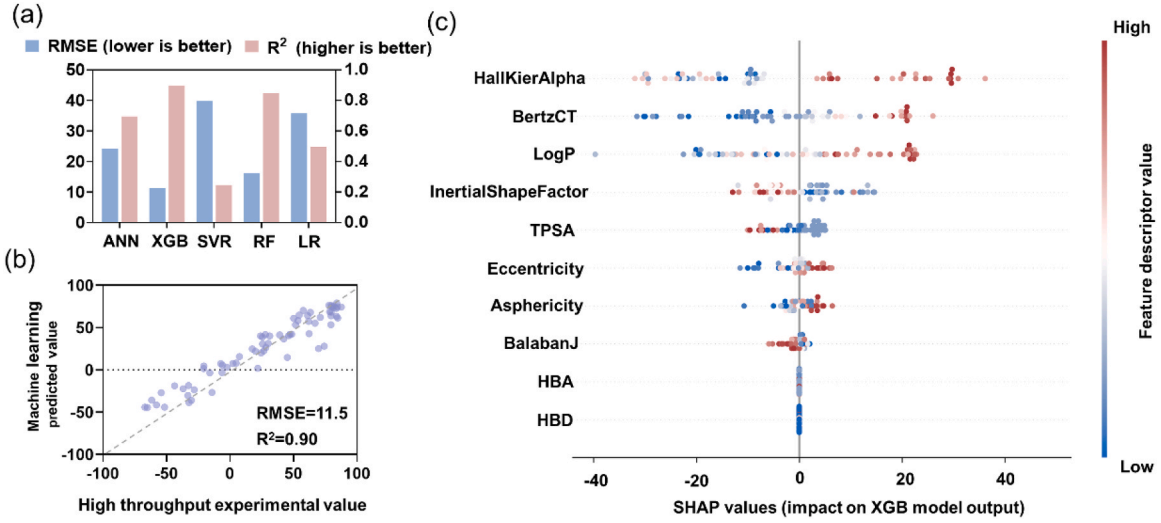

Fig. 4. (a) The RMSE and R^2 values for ANN, XGB, SVR, RF, and LR models. (b) Distribution of predicted values using the best machine learning model (XGB). (c) Summary of the SHAP values (impact on XGB model output) of each feature descriptor related to the corrosion inhibition behavior via a bee swarm diagram. Each point corresponded to a unique experimental value, and the position of points showed the impact of a feature descriptor on predicted IDcorr values.

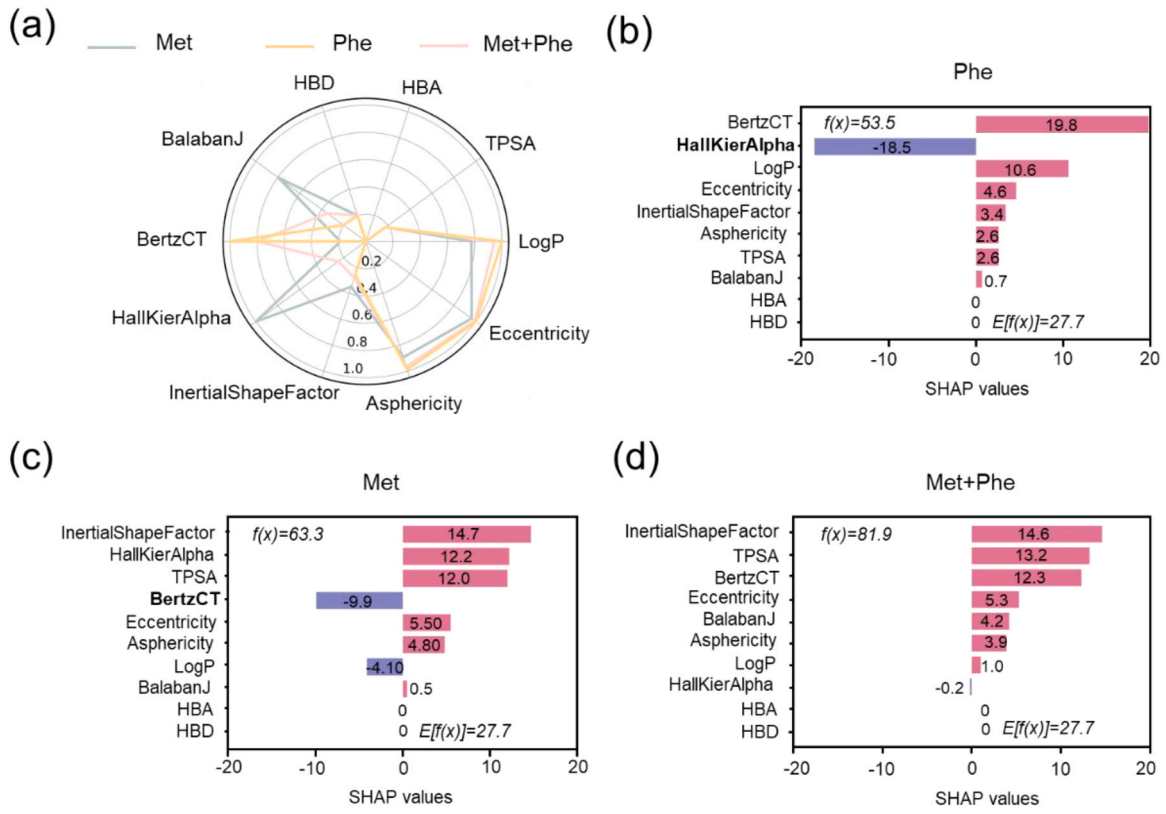

Fig. 5. (a) Normalized feature descriptor values for Phe, Met, and Met+Phe samples. The SHAP values of each feature descriptor for (b) Phe, (c) Met, and (d) Met+Phe samples. f(x) (top left) represented the IDcorr value of the single sample while E[f(x)] (lower right) represented the mean IDcorr value of the data set.

In order to explain the underlying correlations between the molecular feature descriptors and the corrosion inhibition performance, we used the SHAP analysis to provide an intuitive way to interpret the output (IDcorr values) of the XGB model (see Section 2.4). The sum of the SHAP values for its feature descriptors is simply equal to the difference between the predicted value of this sample and the average predicted value of all samples in the data set. A bee swarm diagram was used to summarize the SHAP values of the feature descriptors related to the corrosion inhibition behavior (Fig. 4**c**). The red and blue colors indicated that values of the feature descriptors of this sample were relatively high or lower in all samples, respectively. The values of abscissa were determined by the magnitude of SHAP values of the descriptors. The distribution of SHAP values for the selected features except hydrogen bond features is relatively wide and monotonic overall, which indicated that all descriptors except hydrogen bond features had a significant effect on the corrosion inhibition of molecules. Among these, two 2D molecular graph descriptors, HallKierAlpha, and BertzCT, exhibited the strongest correlations to the inhibition performance of amino acid molecules. HallKierAlpha value was obtained by calculating the electron density around each atom, which could capture direct electronic interactions and charge distribution of molecules [51]. The molecule with a high HallKierAlpha value had a high possibility to donate electrons. This value was positively related to the inhibition performance of amino acid molecules. BertzCT was a topological index to quantify the complexity of bond connectivity in molecular graphs. In general, a high BertzCT value reflects a high bond order. Bond order was calculated by the number of electron pairs shared between atoms [52]. Therefore, the molecule with a high BertzCT value tended to accept electrons, which was positively correlated to the inhibition performance. Note that 3D shape descriptors seemed to have a lower impact on amino acid corrosion inhibition behavior compared to 2D molecular graph descriptors. This could be explained by the relatively simple 3D structures in low molecular weight amino acids [47]. Although the values of hydrogen bond descriptors were variational for amino acid molecules, they were all computed with 0 SHAP value. These results indicated that the hydrogen bonds of amino acid molecules were not the main factor influencing their corrosion inhibition performance. This finding agrees with the work reported previously, which showed that the formation of hydrogen bonds contributed little to the inhibitory action without the presence of a passive film on the metal surface [32]. A passive film may indeed not be present under our experimental conditions (carbon steel in HCl solution).

To further understand the enhanced corrosion inhibition performance of Met+Phe inhibitors, the SHAP values of the feature descriptors for Phe, Met, and Met+Phe samples were computed. The normalized feature descriptor values were shown in Fig. 5a while the SHAP values of the descriptors were shown in Fig. 5b–d. The inadequate corrosion inhibition capacity of Phe was attributed to its low HallKierAlpha value (−1.35). This could be evidenced by the extremely negative SHAP value of HallKierAlpha for the Phe sample. On the contrary, although the HallKierAlpha (−0.22) value of Met was high and it was demonstrated to exhibit positive contributions, the low BertzCT (96.96) value with the negative SHAP values may hinder its inhibition performance (Fig. 5c). These results indicated that HallKierAlpha and BertzCT were the critical features determining the inhibition behavior for single Phe or Met samples. When Phe and Met were used in combination, the HallKierAlpha value of the samples significantly increased while their relatively high BertzCT value was maintained (Fig. 5a). The BertzCT was still positively related to the performance of Met+Phe samples. The negative effect of HallKierAlpha disappeared (Fig. 5d). As mentioned above, HallKierAlpha and BertzCT values could reflect the electron donation and acceptance tendency of amino acid molecules, respectively. Therefore, Met+Phe samples possessed a strong capacity for both electron donation and acceptance, exhibiting stronger interaction with steel surfaces compared to single Met or Phe. This interaction culminated in the formation of a denser barrier film, which led to their observed

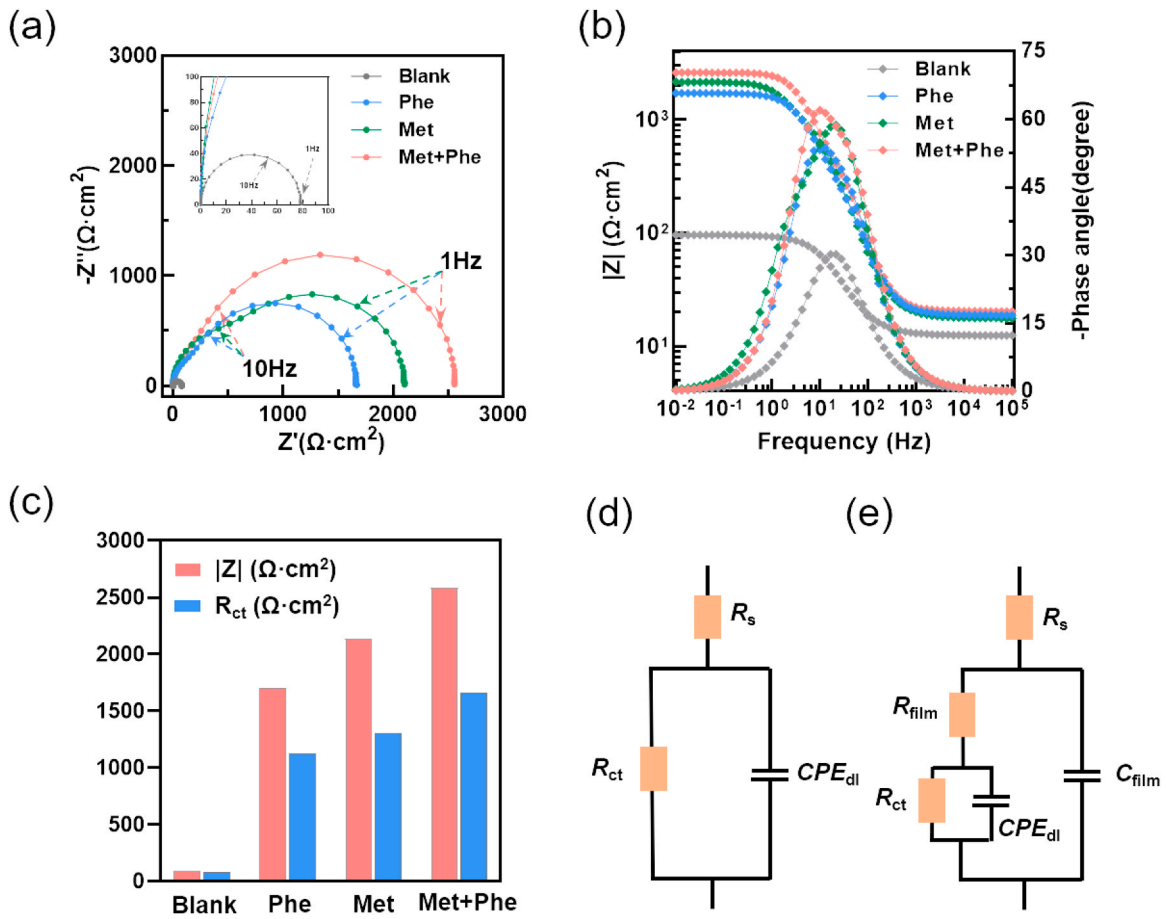

Fig. 6. (a) Nyquist diagrams and (b) Bode plots of carbon steel in 0.1 M HCl solution without and with Phe, Met, and Met+Phe corrosion inhibitors after 24 hours of immersion. (c) $|Z|_{0.01\ Hz}$ and fitted R_{ct} values of carbon steels exposed to 0.1 M HCl solution or different amino acid corrosion inhibitor solutions. The electrical equivalent circuit used to fit the data of (d) blank HCl solution samples and (e) amino acid corrosion inhibitor samples.

optimal corrosion inhibition performance in the experiments. In order to assess the recognition ability of this method for the interactions in different amino acid mixtures, the enhanced corrosion inhibition performance of Leu+Phe samples was also investigated. The negative contributions of HallKierAlpha and BertzCT for Phe and Leu samples were reversed to be positive for Phe+Leu mixtures, respectively (Fig. S2). This explains the enhanced corrosion inhibition performance of Leu+Phe sample in the experiments. The lower value of HallKierAlpha in Leu than that in Met is responsible for weaker corrosion inhibition enhancement of the Leu+Phe sample than that of Met+Phe sample in the experiments.

3.4. Electrochemical verification

EIS was used to verify the corrosion inhibition performance of the optimal amino acid. Fig. 6a and 6b showed the Nyquist and Bode plots of Q235 steel with different amino acid corrosion inhibitors after 24 hours of immersion, respectively. In the Nyquist plots, the blank solution showed a single semicircular capacitive loop with a small diameter. In the presence of amino acids, the diameters of the capacitive loop all increased. The depression of the semicircles represented the emergence of two overlapped capacitive loops. Compared to Met or Phe, the diameter of the capacitive loop in the Met+Phe mixture further increased. The diameter was generally believed to represent the charge transfer resistance [53]. For the Bode plots, the order of the low-frequency impedance modulus at 0.01 Hz ($|Z|_{0.01\ Hz}$) was Met+Phe > Met > Phe > Blank, in agreement with the results of the Nyquist plots (Fig. 6**c**). In the phase angle plots, the break point frequency of the Met+Phe sample shifted to a lower value compared to that of single Met or Phe samples. This shift is directly related to inhibitor adsorption at the metal surface and the diversities of dielectric features. The changes in dielectric features resulted from the adsorptions of water molecules and ions on the surfaces induced by the introduction of amino acid molecules [54]. Moreover, the phase angle value of the Met+Phe sample was the highest, indicating the enhanced adsorption of the mixtures at the metal-solution interface [55].

Table 5
Fitted equivalent circuit parameters for EIS data. Data are means ± SD (n = 3, SD indicates standard deviation).

Samples	R_s	CPE_{dl}	R_{ct}		CPE_{film}		R_{film}	$Chsq$
	($\Omega\cdot cm^{-2}$)	($\mu\Omega^{-1}\cdot S^{n}\cdot cm^{-2}$)	n	($\Omega\cdot cm^{-2}$)	($\mu\Omega^{-1}\cdot S^{n'}\cdot cm^{-2}$)	n'	($\Omega\cdot cm^{-2}$)	10^{-4}
Blank	12.4 ± 1.1	315.4 ± 18.2	0.83 ± 0.04	84 ± 18	—	—	—	—
Phe	18.7 ± 1.2	30.3 ± 2.0	0.92 ± 0.02	1128 ± 26	20.5 ± 2.6	0.93 ± 0.01	566 ± 17	4.82
Met	17.6 ± 2.1	98.8 ± 4.5	1	1303 ± 30	25.7 ± 2.3	0.91 ± 0.02	826 ± 23	4.33
Met+Phe	20.2 ± 0.6	15.4 ± 1.4	1	1661 ± 31	14.1 ± 1.9	0.96 ± 0.01	916 ± 18	6.49

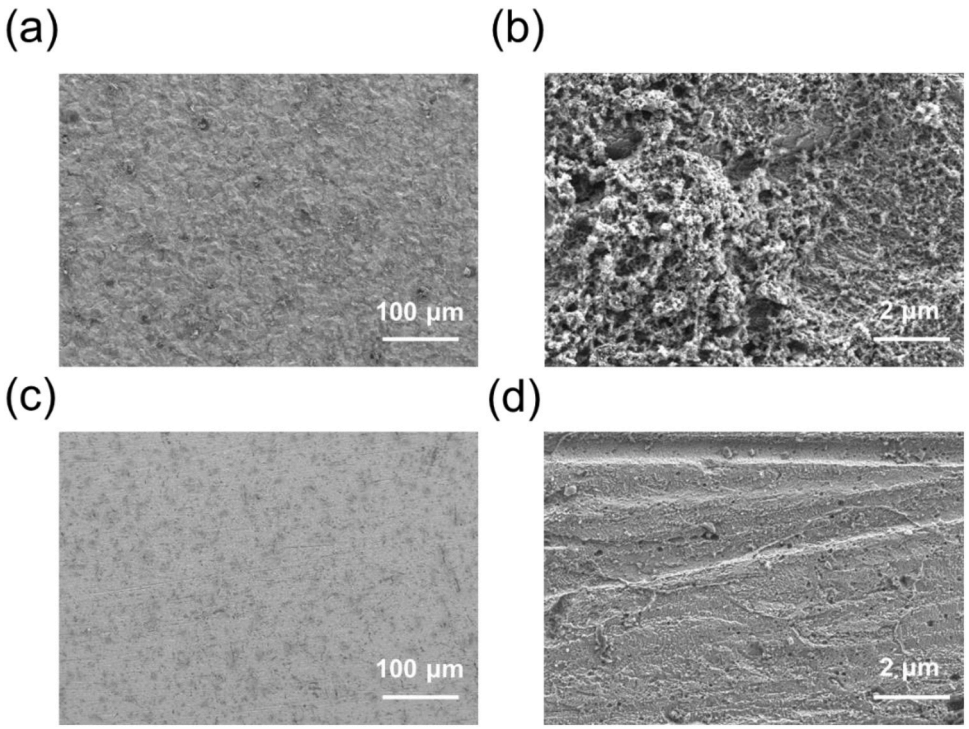

Fig. 7. SEM images of carbon steels in 0.1 M HCl solution (a, b) without and (c, d) with Met+Phe corrosion inhibitor after 24 hours of immersion.

Subsequently, equivalent circuit models shown in Fig. 6d and e were used to fit the EIS data for blank and amino acid samples, respectively. The R_s, R_{film}, and R_{ct} represented the solution resistance, film resistance, and charge transfer resistance, respectively. CPE_{dl} was the constant phase element of double layer capacitance, while CPE_{film} meant the film capacitance of the adsorbed inhibitors [27,56]. Chi-square values were used to evaluate the fit goodness of the equivalent circuit models, which ranged from 4.33×10^{-4} to 6.49×10^{-4} [57]. The fitted parameters were shown in Table 5 while the R_{ct} values were exhibited in Fig. 6**c**, indicating the corrosion rate of the metal surface. A larger R_{ct} value reflects a slower corrosion rate [58]. Consistent with the results for low-frequency impedance moduli, the fitted R_{ct} values were in the order of Met+Phe > Met > Phe > Blank. Therefore, Met+Phe samples exhibited the optimal corrosion inhibitor performance. According to the literature [59,60], the thickness of the adsorption film of amino acid inhibitors could be calculated by Eq. (5) and Eq. (6):

$$C_{film} = CPE_{film}^{1/n'}(R_s^{-1}+R_{film}^{-1})^{(n'-1)/n'} \quad (5)$$

$$d_{film}=\varepsilon_0\varepsilon A/C_{film} \quad (6)$$

where C_{film} is the capacitance. ε_0 and ε are the permittivity of the media and the local dielectric constant, respectively. d_{film} is the film thickness, and A is the geometric area of the electrode (1 cm^2). For the thin films, the ε value of the dielectric constant is assumed between 10 and 20 [61, 62]. Therefore, the thickness of the adsorption film of Met+Phe sample was calculated to be between 0.90 and 1.80 nm. SEM images were used to intuitively assess the actual protective effect of the adsorption film of Met+Phe sample (Fig. 7). As shown in Fig. 7a and b, carbon steel surfaces without corrosion inhibitors exhibited serious corrosion. The visible corrosion products were unevenly distributed and accumulated on the metal surface. On the contrary, the carbon steel showed a much higher surface flatness and homogeneity with the addition of Met+Phe samples (Fig. 7c, d). The corrosion process of the carbon steel was significantly alleviated. Moreover, we noticed that the R_s value of amino acid samples was higher than that of the blank sample. This could be

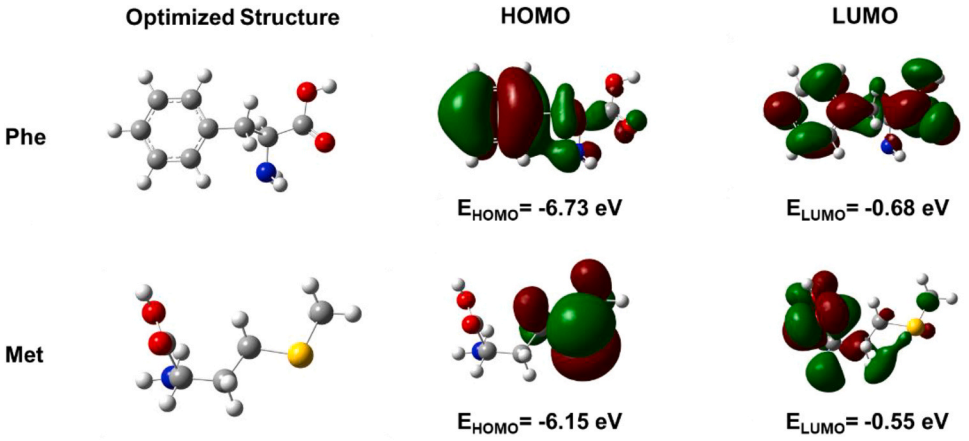

Fig. 8. Optimized structures and the frontier molecule orbital distributions of Phe and Met molecules.

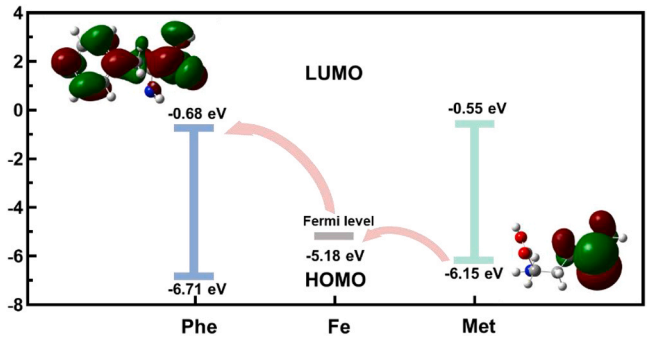

Fig. 9. E_{HOMO} and E_{LUMO} values of Phe and Met molecules, and the electron transfer tendency from Met+Phe samples to metal surfaces.

explained by the protonation of amino acid molecules that slightly increased the pH of the HCl solution. Fig. S3 showed the Tafel curves of carbon steel without and with different amino acid corrosion inhibitors after 24 hours of immersion. Compared to Met (14.6 μA·cm^{-2}) and Phe (17.3 μA·cm^{-2}) samples, the Met+Phe sample further reduced the I_{corr} values (7.7 μA·cm^{-2}) of the steels. The corresponding inhibition efficiency was also increased from ~90 % to ~95 % (Table S1). The above electrochemical results verified the enhanced corrosion inhibition effect using Met and Phe mixtures.

3.5. Quantum chemical calculations of amino acid corrosion inhibitors

Although single quantum chemical parameters may exhibit insufficient general correlations to the inhibition efficiencies of corrosion inhibitors [63,64], they provide information of the electron transfer between amino acid molecules and metal surfaces [3,13,65]. Therefore, quantum chemical calculations were performed to verify the corrosion inhibition behavior of Met+Phe samples. The optimized structures and frontier molecule orbital distributions of Phe and Met molecules were shown in Fig. 8. For Phe, the HOMO is mainly localized on the benzene ring and the LUMO is distributed at the entire molecule. For Met, the HOMO existed on the skeleton containing the sulphur atom, while the LUMO was primarily distributed at the carboxyl group. The eigenvalue of the HOMO (E_{HOMO}) was positively correlated with the possibility to donate electrons, and the eigenvalue of the LUMO (E_{LUMO}) was negatively correlated with the capacity to accept electrons [66]. Met shows a stronger ability to donate electrons, while Phe is likely to accept electrons. The electron transfer between inhibitor molecules and steel surfaces depended on the E_{HOMO} and E_{LUMO} of the inhibitor molecules and the Fermi level of Fe ($E_{F,\ Fe}$) [19]. The E_{HOMO} of Met (−6.15 eV) was closer to the $E_{F,\ Fe}$ (−5.18 eV) compared to that of Phe (−6.71 eV) (Fig. 9). This result indicated that the electrons were more possible to be excited from the HOMO of Met to the carbon steel surface. Phe (−0.68 eV) exhibited a closer E_{LUMO} to $E_{F,\ Fe}$ (−5.18 eV) than Met (−0.55 eV), indicating that electrons tended to transfer from the steel surface to the LUMO of Phe. Therefore, compared to the situation of single Met or Phe, electron transfer between the HOMO of Met and the steel surface and between the steel surface and the LUMO of Phe is increasingly facilitated when Met and Phe were used in combination. These results demonstrated that Met+Phe samples simultaneously exhibited enhanced electron donation and acceptance capacity, which supported the synergistic mechanism obtained by machine learning analysis (see Section 3.3).

4. Conclusion

In summary, we proposed an advanced methodology to integrate high-throughput experiments and interpretable machine learning technology to identify the corrosion inhibition synergism of amino acid combinations. A corrosion inhibitor library with labeled data of 70 amino acid formulations was effectively created by the automated configurations of large amount of amino acid solutions and color responses based on Fe ions generated during the corrosion process. The results of high-throughput experiment demonstrated significantly enhanced inhibition performance when 25 % Met and 75 % Phe were used in combination. Benefiting from the creation of amino acid library, an interpretable machine learning technology was used to grasp the underlying correlations between various amino acid molecular features and the experimentally obtained IDcorr values. SHAP analyses with the XGB model computed the marginal contributions of various feature descriptors of amino acid molecules to the predicted inhibition behavior. Machine learning results revealed that all descriptors except hydrogen bond features had a significant effect on the corrosion inhibition of amino acid molecules. Moreover, Met+Phe samples exhibit high HallKierAlpha and BertzCT values, exhibiting a strong capacity for both electron donation and acceptance. The augmented interaction of Met+Phe samples and carbon steel led to the observed inhibition enhancement. This synergistic effect of Met+Phe samples was well supported by electrochemical tests and quantum chemical calculations. The proposed methodology could be helpful for understanding the contribution of different molecular features to inhibition performance of corrosion inhibitors and the synergisms in the optimal formulation. Notably, the results from interpretable machine learning led to a significantly narrow list of feature descriptor candidates for subsequent exploration via in-depth experiments and theoretical calculations.

CRediT authorship contribution statement

Lingwei Ma: Validation, Supervision. **Hongchang Qian:** Validation, Supervision. **Zhongheng Fu:** Writing – review & editing, Validation. **Yami Ran:** Investigation. **Xin Guo:** Validation. **Junsen Zhao:** Validation, Investigation. **Jingzhi Yang:** Writing – original draft, Methodology, Investigation, Conceptualization. **Dawei Zhang:** Writing – review & editing, Supervision, Conceptualization. **Arjan Mol:** Writing – review & editing, Supervision. **Patrick Keil:** Writing – review & editing, Supervision.

Declaration of Competing Interest

The authors declare no competing financial interests or personal relationships in this paper.

Acknowledgement

This work is financially supported by the Postdoctoral Fellowship Program of CPSF under Grant Number GZC20240101.

Appendix A. Supporting information

Supplementary data associated with this article can be found in the online version at doi:10.1016/j.corsci.2025.112675.

Data Availability

Data will be made available on request.

References

[1] I. Aiad, S.M. Shaban, A.H. Elged, O.H. Aljoboury, Cationic surfactant based on alignate as green corrosion inhibitors for the mild steel in 1.0 M HCl, Egypt. J. Pet. 27 (2018) 877–885.
[2] C.F. Sabel, D.G. Victor, Governing global problems under uncertainty: making bottom-up climate policy work, Clim. Change 144 (2015) 15–27.
[3] A. Farhadian, A. Rahimi, N. Safaei, A. Shaabani, M. Abdouss, A. Alavi, A theoretical and experimental study of castor oil-based inhibitor for corrosion inhibition of mild steel in acidic medium at elevated temperatures, Corros. Sci. 175 (2020) 108871.
[4] P. Wang, J. Wang, Y. Huang, X. Cheng, Z. Zhao, L. Ma, S. Wang, R. Han, Z. Zhang, D. Zhang, X. Li, Effects of grain size on the corrosion inhibition and adsorption

performance of benzotriazole on carbon steel in NaCl solution, J. Mater. Sci. Technol. 217 (2025) 221–236.
[5] Y. Qiang, H. Li, X. Lan, Self-assembling anchored film basing on two tetrazole derivatives for application to protect copper in sulfuric acid environment, J. Mater. Sci. Technol. 52 (2020) 63–71.
[6] B. Hou, Q. Zhang, Y. Li, G. Zhu, Y. Lei, X. Wang, F. Liu, G. Zhang, In-depth insight into the inhibition mechanism of pyrimidine derivatives on the corrosion of carbon steel in CO_2-containing environment based on experiments and theoretical calculations, Corros. Sci. 181 (2021) 109236.
[7] D. Costa, C.-M. Pradier, F. Tielens, L. Savio, Adsorption and self-assembly of bio-organic molecules at model surfaces: a route towards increased complexity, Surf. Sci. Rep. 70 (2015) 449–553.
[8] D. Kumar, N. Jain, V. Jain, B. Rai, Amino acids as copper corrosion inhibitors: a density functional theory approach, Appl. Surf. Sci. 514 (2020) 145905.
[9] T. Stimpfling, P. Vialat, H. Hintze-Bruening, P. Keil, V. Shkirskiy, P. Volovitch, K. Ogle, F. Leroux, Amino acid interleaved layered double hydroxides as promising hybrid materials for AA2024 corrosion inhibition, Eur. J. Inorg. Chem. 19 (2016) 2006–2016.
[10] O. Olivares, N.V. Likhanova, B. Gómez, J. Navarrete, M.E. Llanos-Serrano, E. Arce, J.M. Hallen, Electrochemical and XPS studies of decylamides of α-amino acids adsorption on carbon steel in acidic environment, Appl. Surf. Sci. 252 (2006) 2894–2909.
[11] Q. Zhang, B. Hou, Y. Li, Y. Lei, X. Wang, H. Liu, G. Zhang, Two amino acid derivatives as high efficient green inhibitors for the corrosion of carbon steel in CO_2-saturated formation water, Corros. Sci. 189 (2021) 109596.
[12] C. Zhang, H. Duan, J. Zhao, Synergistic inhibition effect of imidazoline derivative and l-cysteine on carbon steel corrosion in a CO_2-saturated brine solution, Corros. Sci. 112 (2016) 160–169.
[13] Q. Zhang, Y. Li, Y. Lei, X. Wang, H. Liu, G. Zhang, Comparison of the synergistic inhibition mechanism of two eco-friendly amino acids combined corrosion inhibitors for carbon steel pipelines in oil and gas production, Appl. Surf. Sci. 583 (2022) 152559.
[14] C. Ren, L. Ma, X. Luo, C. Dong, T. Gui, B. Wang, X. Li, D. Zhang, High-throughput assessment of corrosion inhibitor mixtures on carbon steel via droplet microarray, Corros. Sci. 213 (2023) 110967.
[15] A.V. Zabula, S. Dey, J.R. Robinson, T. Cheisson, R.F. Higgins, G. Bhargava, R. C. Nahas, D. Cinoman, M. Kerins, E.C. Houze, E.J. Schelter, Screening of molecular lanthanide corrosion inhibitors by a high-throughput method, Corros. Sci. 165 (2020) 108377.
[16] Y. Qiu, X. Tu, X. Lu, J. Yang, A novel insight into synergistic corrosion inhibition of fluoride and DL-malate as a green hybrid inhibitor for magnesium alloy, Corros. Sci. 199 (2022) 110177.
[17] P.A. White, A.E. Hughes, S.A. Furman, N. Sherman, P.A. Corrigan, M.A. Glenn, D. Lau, S.G. Hardin, T.G. Harvey, J. Mardel, T.H. Muster, S.J. Garcia, C. Kwakernaak, J.M. Mol, High-throughput channel arrays for inhibitor testing: Proof of concept for AA2024-T3, Corros. Sci. 51 (2009) 2279–2290.
[18] C. Ren, L. Ma, D. Zhang, X. Li, A. Mol, High-throughput experimental techniques for corrosion research: a review, MGE Adv. 1 (2023) e20.
[19] X. Guo, X. Ding, Y. Wang, J. Wang, W. Tan, Y. Li, Z. Chen, Z. Li, W. Chen, L. Ma, D. Zhang, High-throughput screening of green amino acid and surfactant mixtures with high corrosion inhibition efficiency: experimental and modelling perspectives, Corros. Sci. 240 (2024) 112460.
[20] Q. Zhang, Y. Li, G. Zhu, Y. Lei, X. Wang, H. Liu, G. Zhang, In-depth insight into the synergistic inhibition mechanism of S-benzyl-L-cysteine and thiourea on the corrosion of carbon steel in the CO_2-saturated oilfield produced water, Corros. Sci. 192 (2021) 109807.
[21] V. Shkirskiy, P. Keil, H. Hintze-Bruening, F. Leroux, F. Brisset, K. Ogle, P. Volovitch, The effects of l-cysteine on the inhibition and accelerated dissolution processes of zinc metal, Corros. Sci. 100 (2025) 101–112.
[22] M. Zerfaoui, H. Oudda, B. Hammouti, S. Kertit, M. Benkaddour, Inhibition of corrosion of iron in citric acid media by aminoacids, Prog. Org. Coat. 51 (2004) 134–138.
[23] Y. Zhang, Y. Wu, N. Li, Y. Jiang, Y. Qian, L. Wang, J. Zhang, Synergistic inhibition effect of L-Phenylalanine and zinc salts on chloride-induced corrosion of magnesium alloy: experimental and theoretical investigation, J. Taiwan Inst. Chem. E. 121 (2021) 48–60.
[24] G.K. Gomma, Corrosion inhibition of steel by benzotriazole in sulphuric acid, Mater. Chem. Phys. 55 (1998) 235–240.
[25] M. Sharma, J. Chawla, G. Singh, Cetyl trimethylammonium bromide as corrosion inhibitor for mild steel in acidic medium, Indian J. Chem. Technol. 16 (2009) 339–343.
[26] Q. Deng, S. Jeschke, B.J. Murdoch, S. Hirth, P. Eiden, J.N. Gorges, P. Keil, X. Chen, I. Cole, In-depth insights of inhibitory behaviour of 2-amino-4-methylthiazole towards galvanised steel in neutral NaCl solution, Corros. Sci. 199 (2022) 110206.
[27] N. Tavandashti, M. Ghorbani, A. Shojaei, J. Mol, H. Terryn, K. Baert, Y. Gonzalez-Garcia, Inhibitor-loaded conducting polymer capsules for active corrosion protection of coating defects, Corros. Sci. 112 (2016) 138–149.
[28] H. Gao, Q. Li, Y. Dai, F. Luo, H. Zhang, High efficiency corrosion inhibitor 8-hydroxyquinoline and its synergistic effect with sodium dodecylbenzenesulphonate on AZ91D magnesium alloy, Corros. Sci. 52 (2010) 1603–1609.
[29] E. Rakanta, Th Zafeiropoulou, G. Batis, Corrosion protection of steel with DMEA-based organic inhibitor, Constr. Build. Mater. 44 (2013) 507–513.
[30] E.E. Oguzie, Y. Li, F. Wang, Corrosion inhibition and adsorption behavior of methionine on mild steel in sulfuric acid and synergistic effect of iodide ion, J. Colloid Interf. Sci. 310 (2007) 90–98.
[31] J. Fu, S. Li, Y. Wang, X. Liu, L. Lu, Computational and electrochemical studies on the inhibition of corrosion of mild steel by L-Cysteine and its derivatives, J. Mater. Sci. 46 (2011) 3550–3559.
[32] A. Nautiyal, M. Qiao, J. Cook, X. Zhang, T.-S. Huang, High performance polypyrrole coating for corrosion protection and biocidal applications, Appl. Surf. Sci. 427 (2018) 922–930.
[33] M.A. Amin, K.F. Khaled, Q. Mohsen, H.A. Arida, A study of the inhibition of iron corrosion in HCl solutions by some amino acids, Corros. Sci. 52 (2010) 1684–1695.
[34] M.P. Desimone, G. Gordillo, S.N. Simison, The effect of temperature and concentration on the corrosion inhibition mechanism of an amphiphilic amido-amine in CO_2 saturated solution, Corros. Sci. 53 (2011) 4033–4043.
[35] X. Wang, H. Yang, F. Wang, An investigation of benzimidazole derivative as corrosion inhibitor for mild steel in different concentration HCl solutions, Corros. Sci. 53 (2011) 113–121.
[36] W. Li, D. Li, Influence of surface morphology on corrosion and electronic behavior, Acta Mater. 54 (2006) 445–452.
[37] M. Vijayan, Molecular interactions and aggregation involving amino acids and peptides and their role in chemical evolution, Prog. Biophys. Molec. Biol. 52 (1988) 71–99.
[38] Q. Deng, S. Jeschke, R.K. Mishra, S. Spicher, S. Darouich, E. Schreiner, P. Eiden, P. Deglmann, J.N. Gorges, X. Chen, P. Keil, Ivan Cole, Design of alkyl-substituted aminothiazoles to optimise corrosion inhibition for galvanised steel: a combined experimental and molecular modelling approach, Corros. Sci. 227 (2024) 111733.
[39] A. Kokalj, Considering the concept of synergism in corrosion inhibition, Corros. Sci. 212 (2023) 110922.
[40] Z. Ren, Z. Ren, Z. Zhang, T. Buonassisi, J. Li, Autonomous experiments using active learning and AI, Nat. Rev. Mater. 8 (2023) 563–564.
[41] W. Xie, W. Wang, Y. Liu, On the application of high-throughput experimentationand data-driven approaches in metallic glasses, MGE Adv. 1 (2023) e8.
[42] J. Yang, Y. Ran, S. Liu, C. Ren, Y. Lou, P. Ju, G. Li, X. Li, D. Zhang, Synergistic D-amino acids based antimicrobial cocktails formulated via high-throughput screening and machine learning, Adv. Sci. 11 (2024) 202307173.
[43] J. Zhang, G. Qiao, S. Hu, Y. Yan, Z. Ren, L. Yu, Theoretical evaluation of corrosion inhibition performance of imidazoline compounds with different hydrophilic groups, Corros. Sci. 53 (2011) 147–152.
[44] Y. Qiang, S. Zhang, L. Wang, Understanding the adsorption and anticorrosive mechanism of DNA inhibitor for copper in sulfuric acid, Appl. Surf. Sci. 492 (2019) 228–238.
[45] H. Assad, A. Kumar, Understanding functional group effect on corrosion inhibition efficiency of selected organic compounds, J. Mol. Liq. 344 (2021) 117755.
[46] T.G. Harvey, S.G. Hardin, A.E. Hughes, T.H. Muster, P.A. White, T.A. Markley, P. A. Corrigan, J. Mardel, S.J. Garcia, J.M.C. Mol, A.M. Glenn, The effect of inhibitor structure on the corrosion of AA2024 and AA7075, Corros. Sci. 53 (2011) 2184–2190.
[47] J. Ma, J. Dai, X. Guo, D. Fu, L. Ma, P. Keil, A. Mol, D. Zhang, Data-driven corrosion inhibition efficiency prediction model incorporating 2D–3D molecular graphs and inhibitor concentration, Corros. Sci. 222 (2023) 112038.
[48] D. Weininger, SMILES, a chemical language and information system. 1. Introduction to methodology and encoding rules, J. Chem. Inf. Comput. Sci. 28 (1988) 31–36.
[49] RDKit: Open-source cheminformatics.⟨www.rdkit.org⟩.
[50] A. Tiihonen, S.J. Cox-Vazquez, Q. Liang, M. Ragab, Z. Ren, N.T.P. Hartono, Z. Liu, S. Sun, C. Zhou, N.C. Incandela, J. Limwongyut, A.S. Moreland, S. Jayavelu, G. C. Bazan, T. Buonassisi, Predicting antimicrobial activity of conjugated oligoelectrolyte molecules via machine learning, J. Am. Chem. Soc. 143 (2021) 18917–18931.
[51] S. Li, Y. Huang, L. Zhang, Accelerated design of stable halide perovskite heterostructure film in hostile condition via surface modifier, Org. Electron. 124 (2024) 106945.
[52] K.M. Toots, S. Sild, J. Leis, W.E. Acree, Jr, U. Maran, The quantitative structure–property relationships for the gas-ionic liquid partition coefficient of a large variety of organic compounds in three ionic liquids, J. Mol. Liq. 343 (2021) 117573.
[53] Y. Zhu, M.L. Free, G. Yi, Electrochemical measurement, modeling, and prediction of corrosion inhibition efficiency of ternary mixtures of homologous surfactants in salt solution, Corros. Sci. 98 (2015) 417–429.
[54] J.O.'M. Bockris, A.K.N. Reddy, M. Gamboa-Aldeco. Modern Electrochemistry, second ed., Kluwer Academic/Plenum Publishers, New York, 2000.
[55] S. Gokmen, T. Tunc, M. Erbil, Assessment of the inhibition efficiency of 3, 4-diaminobenzonitrile against the corrosion of steel, Corros. Sci. 102 (2016) 437–445.
[56] G. Mendonc, S. Costa, V. Freire, P. Casciano, Adriana Correia, P. Lima-Neto, Understanding the corrosion inhibition of carbon steel and copper in sulphuric acid medium by amino acids using electrochemical techniques allied to molecular modelling methods, Corros. Sci. 115 (2017) 41–55.
[57] G. Liu, Y. Zhang, M. Wu, R. Huang, Study of depassivation of carbon steel in simulated concrete pore solution using different equivalent circuits, Constr. Build. Mater. 157 (2017) 357–362.
[58] K.A. Yasakau, A. Kuznetsova, H.M. Maltanava, S.K. Poznyak, M.G.S. Ferreira, M. L. Zheludkevich, Corrosion protection of zinc by LDH conversion coatings, Corros. Sci. 229 (2024) 111889.
[59] G. Brug, A. Van den Eeden, M. Sluyters-Rehbach, J.H. Sluyters, The analysis of electrode impedances complicated by the presence of a constant phase element, J. Electro Chem. 176 (1984) 275–295.

[60] B. Hirschorn, M.E. Orazem, B. Tribollet, V. Vivier, I. Frateur, M. Musiani, Determination of effective capacitance and film thickness from constant-phase-element parameters, Electrochim. Acta 55 (2010) 6218–6227.
[61] M. Finšgar, D.K. Merl, The analysis of electrode impedances complicated by the presence of a constant phase element, Corros. Sci. 98 (2015) 417–429.
[62] M. Finšgar, S. Peljhan, A. Kokalj, J. Kovač, I. Milošev, Determination of the Cu_2O thickness on BTAH-inhibited copper by reconstruction of auger electron spectra determination of effective capacitance and film thickness from constant-phase-element parameters, J. Electrochem. Soc. 157 (2010) C295.
[63] A. Kokalj, M. Lozinšek, B. Kapun, P. Taheri, S. Neupane, P. Losada-Pérez, C. Xie, S. Stavber, D. Crespo, F.U. Renner, A. Mol, I. Milošev, Simplistic correlations between molecular electronic properties and inhibition efficiencies: Do they really exist? Corros. Sci. 179 (2021) 108856.
[64] A. Kokalj, On the alleged importance of the molecular electron-donating ability and the HOMO–LUMO gap in corrosion inhibition studies, Corros. Sci. 180 (2021) 109016.
[65] D. Legut, A.P. Kądzielawa, P. Pánek, K. Marková, P. Váňová, K. Konečná, Š. Langová, Inhibition of steel corrosion with imidazolium-based compounds-Experimental and theoretical study, Corros. Sci. 191 (2021) 109716.
[66] L. Ma, D. Xu, S. Wu, X. Guo, T. Liu, M. Wei, J. Wang, Z. Chen, D. Zhang, Polyurethane coatings with corrosion inhibition and color-fluorescence damage reporting properties based on APhen-grafted carbon dots, Corros. Sci. 232 (2024) 112038.